Bioorganic Chemistry 83 (2019) 277–288

Contents lists available at ScienceDirect

Bioorganic Chemistry

journal homepage: www.elsevier.com/locate/bioorg

Molecular-docking-guided design and synthesis of new IAA-tacrine hybrids as multifunctional AChE/BChE inhibitors

Zhi-Qiang Cheng[a,1], Kong-Kai Zhu[a,b,1], Juan Zhang[a,1], Jia-Li Song[a], Luis Alexandre Muehlmann[c,d], Cheng-Shi Jiang[a,*], Chang-Liang Liu[e,f,*], Hua Zhang[a,*]

[a] School of Biological Science and Technology, University of Jinan, Jinan 250022, China
[b] Shanghai Institute of Materia Medica, Chinese Academy of Sciences, Shanghai 201203, China
[c] Institute of Biological Sciences, University of Brasília, Brasilia 70910900, Brazil
[d] Faculty of Ceilandia, University of Brasília, Brasilia 72220275, Brazil
[e] Cambrian Discovery Inc., Dover, MA 02115, USA
[f] Department of Neurobiology, Harvard Medical School, Boston, MA 02115, USA

ARTICLE INFO

Keywords:
Alzheimer's disease
IAA-tacrine hybrids
Dual AChE/BChE inhibitor
Molecular docking
Neural network electrical activity

ABSTRACT

A series of new indole-3-acetic acid (IAA)-tacrine hybrids as dual acetylcholinesterase (AChE)/butyrylcholinesterase (BChE) inhibitors were designed and prepared based on the molecular docking mode of AChE with an IAA derivative (**1a**), a moderate AChE inhibitor identified by screening our compound library for anti-Alzheimer's disease (AD) drug leads. The enzyme assay results revealed that some hybrids, e.g. **5d** and **5e**, displayed potent dual *in vitro* inhibitory activities against AChE/BChE with IC_{50} values in low nanomolar range. Molecular modeling studies in tandem with kinetic analysis suggest that these hybrids target both catalytic active site and peripheral anionic site of cholinesterase (ChE). Molecular dynamic simulations and Molecular Mechanics/Poisson-Boltzmann Surface Area (MM-PBSA) calculations indicate that **5e** has more potent binding affinity than hit **1a**, which may explain the stronger inhibitory effect of **5e** on AChE. Furthermore, their predicted pharmacokinetic properties and *in vitro* influences on mouse brain neural network electrical activity were discussed. Taken together, compound **5e** can be highlighted as a lead compound worthy of further optimization for designing new anti-AD drugs.

1. Introduction

Alzheimer's disease (AD) is a multifaceted neurodegenerative disorder featured by loss of memory, progressive deficits in cognitive functions and severe behavioral abnormalities [1]. Approximately 46.8 million people worldwide are now believed to suffer from AD, and this number is expected to triple by 2050 with the aging of global population [2].

The pathogenesis of AD involves several pathways including deficiency in cholinergic neurotransmission, beta-amyloid (Aβ) protein and tau protein phosphorylation pathways.1 The recently causal treatment of AD by developing Aβ monoclonal antibodies, Aβ aggregation inhibitors or tau aggregation inhibitors have proven to be unsuccessful [3], while enhancing cholinergic neurotransmission in the brain by increasing the level of acetylcholine (ACh), as symptomatic drug therapy, is currently the most efficacious approach for AD treatment [4]. ACh in the brain is mainly hydrolyzed by cholinesterase (ChE), and thus inhibition of ChE has been proved to be an effective way for the treatment of AD. There are two types of ChE in the nervous system: acetylcholinesterase (AChE) and butyrylcholinesterase (BChE) [5]. Compared with BChE, AChE is 10^{13} folds more active and accounts for nearly 80% ACh hydrolysis in the brain [6]. Four AChE inhibitors including tacrine, donepezil, galantamine, and rivastigmine (Fig. 1) have been approved by FDA [7]. These AChE inhibitors are beneficial to improving memorial and cognitive functions of AD patients, but tacrine was withdrawn from clinical in the US in 2013 due to its hepatotoxicity [8], and others clinically used drugs cannot cure or stop the progress of AD [9]. Studies indicate that the level and activity of BChE rise with AD progression while the AChE activity declines [10]. Moreover, the AChE-knockout mice with normal level and localization of BChE can survive, which supports the idea that BChE compensates the function of AChE [8,11]. Additional inhibition on BChE is therefore considered to

* Corresponding authors at: Cambrian Discovery Inc., Dover, MA 02115, USA (C.L. Liu).
E-mail addresses: jiangchengshi-20@163.com (C.-S. Jiang), Changliang_Liu@hms.harvard.edu (C.-L. Liu), bio_zhangh@ujn.edu.cn (H. Zhang).
[1] These authors contributed equally to this work.

https://doi.org/10.1016/j.bioorg.2018.10.057
Received 28 August 2018; Received in revised form 26 October 2018; Accepted 27 October 2018
Available online 29 October 2018

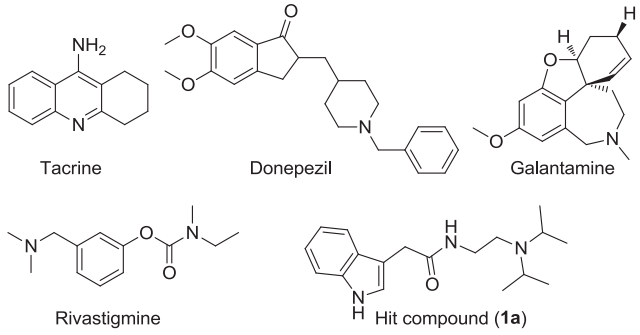

Fig. 1. Structures of AChE inhibitors approved for AD treatment and hit **1a**.

contribute to ameliorating a cholinergic deficit, and dual inhibition of AChE/BChE represents a promising therapeutic strategy for AD treatment [12]. Such dual-targeted ChE inhibitors have shown positive outcomes for the treatment of AD [13,14]. For example, rivastigmine (Fig. 1), as dual AChE/BChE inhibitor, displays more potent effect than donepezil [5].

In the course of our research for developing new anti-AD lead compounds [15,16], an indol-3-acetic acid (IAA) derivative (**1a**, Fig. 1) showing moderate to weak anti-ChE activity was identified. Interestingly, this compound did not show obvious cytotoxicity against HepG2 cells even up to 400 μM, indicating that **1a** serves as a potential anti-ChE lead. In the current study, we carried out further structural modifications of **1a** via two steps, which resulted in a panel of IAA-tacrine hybrids (**5a–5g**) [17] as a new class of potent multifunctional AChE/BChE inhibitors. First, molecular-docking-guided design and synthesis of these new IAA-tacrine AChE/BChE inhibitors, and their inhibitory activities and kinetic analysis were described. Then the preliminary structure-activity relationship (SAR) was discussed, and the binding modes of these hybrids to AChE and BChE were predicted by molecular docking and molecular dynamics simulation. In addition, the pharmacokinetic profiles (solubility, absorption, BBB properties, etc.) and the effect of **5e** on mouse brain neural network electrical activity were described. (See Fig. 2)

2. Results and discussion

2.1. Chemistry

A common feature of numerous ChE inhibitors' structures is the presence of basic nitrogen atom which can be protonated to form cation-π interactions with aromatic amino acid residues in the active pocket of the enzymes [18,19]. Thus, to obtain the preliminary SAR and improve ChE inhibitory activity, several analogues of **1a** were initially prepared with different amino side chain or structural similar side chain as the substitution of -N(iPr)$_2$. The synthetic route for **1a** analogues was depicted in Scheme 1, in which analogues **1a–1p** (Table 1) were prepared by coupling IAA and corresponding amines in the presence of 1-ethyl-3-(3-dimethyllaminopropyl)carbodiimide hydrochloride (EDCI) and 1-hydroxybenzotriazole (HOBT) [20,21].

Next, another batch of IAA-tacrine hybrids **5a–5g** was prepared according to the synthetic route shown in Scheme 2. Briefly, the

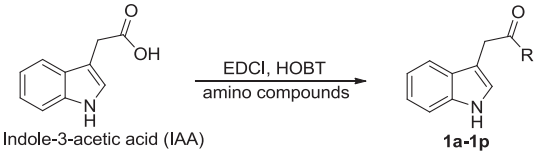

Scheme 1. Synthetic route of analogues **1a–1p**.

reduction of 2-nitrobenzoic acid provided compound **2** which was then condensed with cyclohexanone in the presence of $POCl_3$ under reflux to yield compound **3** [22,23]. The reaction of **3** with different diamines in refluxing pentanol afforded the corresponding intermediates **4a–4g** [24]. Finally, the amidation reaction [17,25] of **4a–4g** with IAA yielded the target compounds **5a–5g** (Table 2). The chemical structures of total twenty-three IAA derivatives were confirmed by ^{1}H, ^{13}C NMR, and MS data.

2.2. In vitro inhibition of AChE and BChE, and SAR study

The AChE and BChE inhibitory activities of all the synthesized compounds were evaluated *in vitro*, with tacrine as positive control. From Table 1, all the analogues **1b–1p** showed no (IC_{50} > 100 μM) or increased ChE inhibitory activity compared with hit **1a**. Among them, only one compound **1n** with the same terminal -N(iPr)$_2$ group as **1a** displayed weak AChE inhibition (IC_{50} = 54.05 ± 3.52 μM). Thus, **1a** was selected as a model compound for further structural modification using computer-aided drug design (CADD) approach.

Firstly, the binding mode of **1a** to AChE was obtained by molecular docking with bis-tacrine dimer (**AA7**)-AChE complex (ID: 5EI5). Analyses of docking result in Fig. 3 revealed that compound **1a** bound well to the active-site gorge of AChE, with partial space superposition with the tacrine moiety in dimer **AA7**. Tacrine has been reported to show excellent inhibition against both AChE and BChE with IC_{50} values at nanomolar level, and there has been a great interest in designing tacrine-based dual binding site ChE inhibitors [25–27]. Based on the binding mode of **1a** in comparison with **AA7**, the terminal -N(iPr)$_2$ group was then modified by fusion with tacrine pharmacophore to improve its activity. In addition, the effect of alkyl diamino chain length was investigated to find the optimal distance between indole and tacrine moieties. In the end, a series of hybrids **5a–5g** were prepared and evaluated for their ChE inhibitory activity.

As shown in Table 1, this class displayed better results with much stronger ChE inhibitory activity than the **1a** series. For example, the AChE inhibitory activity was increased by 38-fold (**5e** vs **1a**), while the BChE inhibitory activity was enhanced more significantly (**5d** and **5e** vs **1a**). Clearly, this improvement should be related to the insertion of tacrine moiety. In AChE bioassay, compound **5e** with 6-carbon aliphatic spacer in the linker showed the best activity with an IC_{50} value of 0.173 μM, similar to that of tacrine. The SAR study revealed that the activity increased with elongation of the diamine linker (from **5a** to **5e**) and then decreased (from **5e** to **5g**), suggesting that 6-carnon diamino was the optimal distance between IAA and tacrine. From the results of BChE inhibitory assay, **5c–5e** exhibited the most potent activity with IC_{50} values ranging from 0.057 to 0.076 μM, better than tacrine.

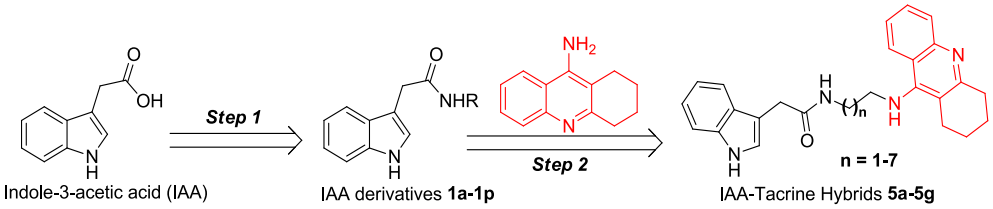

Fig. 2. Structural modifications of IAA.

Table 1
Structures and ChE inhibitory activities of **1a–1p** and **5a–5g.**

Compound	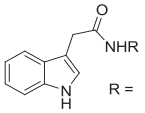	IC_{50}, μM	
		AChE	BChE
1a	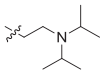	6.62 ± 0.51	98.83 ± 1.78
1b		> 100[a]	> 100
1c		> 100	> 100
1d	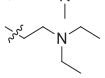	> 100	> 100
1e	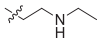	> 100	> 100
1f	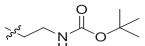	> 100	> 100
1g	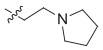	> 100	> 100
1h	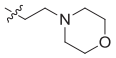	> 100	> 100
1i		> 100	> 100
1j	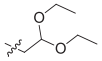	> 100	> 100
1k		> 100	> 100
1l	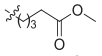	> 100	> 100
1m	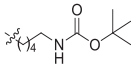	> 100	> 100
1n	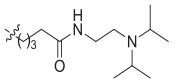	54.05 ± 3.52	> 100
1o	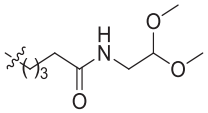	> 100	> 100
1p	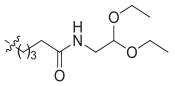	> 100	> 100
5a	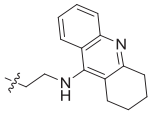	1.665 ± 0.142	0.105 ± 0.022
5b	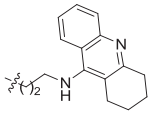	0.998 ± 0.023	0.113 ± 0.051
5c	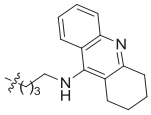	0.395 ± 0.010	0.076 ± 0.004
5d	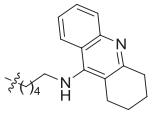	0.264 ± 0.008	0.057 ± 0.008
5e	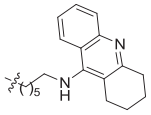	0.173 ± 0.012	0.066 ± 0.003
5f	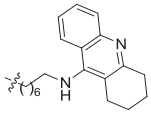	0.376 ± 0.022	0.246 ± 0.028
5g	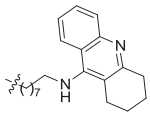	0.353 ± 0.003	0.150 ± 0.021
Tacrine		0.158 ± 0.021	0.268 ± 0.037

[a] IC_{50} value above 100 μM was considered to be inactive.

2.3. Kinetic study of AChE and BChE inhibition

As **5e** displayed potent inhibitory activity toward both AChE and BChE, it was selected as a representative compound for kinetic assay to obtain information on the mode of action and binding site. The mechanisms of AChE and BChE inhibitions were analyzed by recording substrate concentration–enzyme velocity curves in the presence of different concentrations of **5e**.

Graphical analyses revealed both decreasing V_{max} and increasing K_{max} at rising concentrations of **5e** (Figs. 4 and 5). The equilibrium constants for binding with the free enzyme (K_I) and with the enzyme-substrate complex (K_{IS}) were obtained from the slope and the $1/V_{max}$ values plotted against inhibitor concentration, respectively [28]. As shown in Fig. 4, the values of K_I and K_{IS} of **5e** were 0.065 and 0.198 μM for AChE and the estimated K_I and K_{IS} values for BChE were 0.047 and 0.055 μM, respectively (Fig. 5). These patterns indicate that compound **5e** is a linear-mixed type ChE inhibitor ($p < 0.05$) and suggest that **5e** may not only compete with the substrate for the CAS (catalytic active site) but also interact with the second binding site, the PAS (peripheral anionic site). This was in agreement with the subsequent results from molecular modeling study of **5e** (Fig. 6).

2.4. Ligand-protein docking study

Overall, compound **5e** showed the best dual inhibition on AChE and BChE, and was thus selected in the docking simulation. As shown in Figs. 6 and 7, **5e** was able to bind to the active pocket of both AChE and BChE. Regarding AChE, the tacrine moiety of **5e** could spatially overlap with that of **AA7** in the CAS (Fig. 6A), and showed π-π stacking interactions with Trp84 and Phe330 (Fig. 6B). Furthermore, the protonated nitrogen atom in tacrine ring underwent cation-π interaction with Phe330 and formed H-bond with the key residue His440. Although the indole moiety had different orientation at the other end of **AA7** in the PAS (Fig. 6A), it could form π-π stacking interaction with key residue Trp279 and H-bond interaction with Arg289 (Fig. 6B). It was noteworthy that the indole moiety of **5e** and **1a** showed opposite spatial direction in the proposed binding modes. In addition, hydrophobic interactions between **5e** and residues also contributed to the affinity of **5e** to the active site of AChE.

Protein-ligand interactions between **5e** and BChE were shown in Fig. 7. It deserved to mention that the tacrine moiety of **5e** was located in the PAS of BChE [29]. The protonated nitrogen atom of tacrine ring could form H-Bond interaction with Pro265 and cation-π interaction with Tyr 332 of the PAS. The indole moiety could form two types of interactions with key residue Trp82 of the CAS including π-π stacking and hydrophobic interactions, which also highly contributed to the stabilization of the complex. Further, to probe the probable reason why **5e** displayed more potent inhibition activity than tacrine, their binding modes with BChE were compared. As shown in Fig. 8, tacrine overlapped with the indole part of **5e** in the CAS of BChE, which indicated that **5e** had more interactions with BChE than tacrine. In addition, the

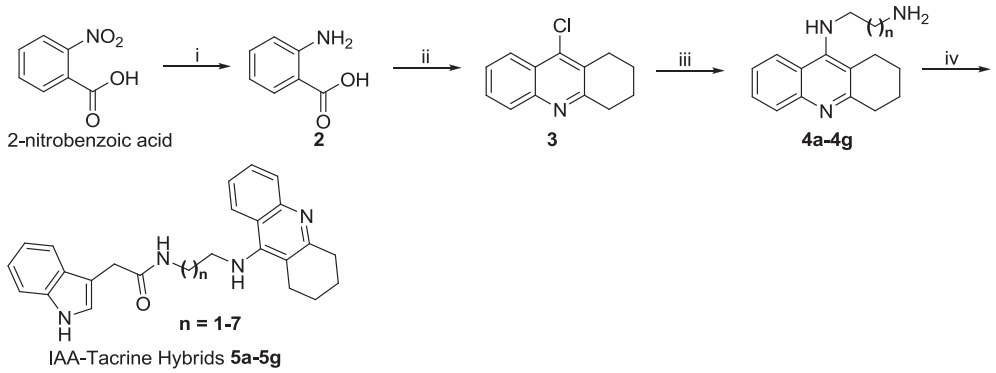

Scheme 2. The general procedure for the synthesis of **5a–5g**. (i): Pd/C (wetted with ca. 55% water), H_2, methanol, r.t.; (ii): $POCl_3$, cyclohexanone, 105 °C, 4 h; (iii): 2- to 8-carbon alkyl diamines, pentanol, 140 °C, 12 h; (iv): IAA, HATU, DIEA, CH_2Cl_2, r.t.

Table 2
Hydrogen bonds existent in the two complexes and their occupancies during the 100 ns MD simulation.

Inhibitors	H-bond Donor	H-bond Acceptor	Occupancy Rate[a]
1a	Tyr121:OH	1a:O1	92.82%
	1a:N3	Tyr70:O	60.46%
5e	Tyr121:OH	5e:O1	41.72%
	5e:N3	Glu199:OE2	99.74%
	5e:N4	Glu278:OE1	64.32%

[a] Only H-bond occupancies > 40% are shown.

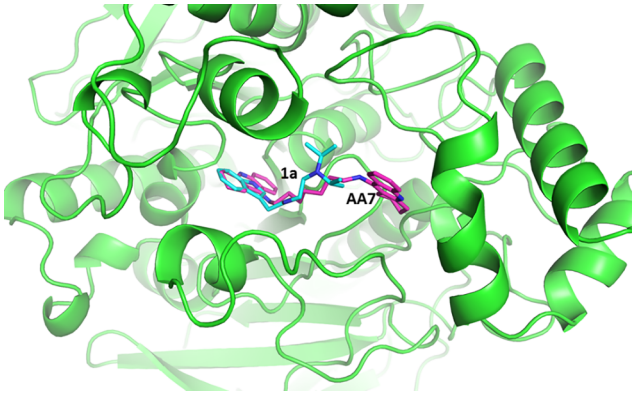

Fig. 3. The proposed binding mode of **1a** (carbon in blue) to AChE. PDB code 5EI5 was used and shown as cartoon, with ligand **AA7** as stick in purple color.

docking score for **5e** and tacrine is −9.30 and −8.50, respectively, which further confirmed the tighter binding of **5e**. Thus, we proposed that the potent inhibition of **5e** resulted from the more tight binding with BChE.

2.5. Molecular dynamics simulation and MM-PBSA calculation

To further probe the molecular mechanism that **5e** showed stronger activity against AChE than **1a**, 100 ns molecular dynamics (MD) simulation and Molecular Mechanics/Poisson-Boltzmann Surface Area (MM-PBSA) calculation were conducted. The time evolution of weighted root-mean-square deviations (RMSDs) for backbone atoms of the AChE protein from their initial positions (t = 0) were calculated. As shown in Fig. 9, RMSDs values of the two complexes were found to be between 0.75 and 1.75 Å in all simulations. Steady RMSD values for the heavy atoms of the protein indicated well-equilibrated states of the systems during MD simulations and showed the reliability of these MD trajectories, suggesting the suitability for post analysis.

H-bonds and hydrophobic interactions in both complexes were analyzed based on MD trajectories (Tables 2 and 3). In the **1a**/AChE complex, two conserved H-bonds between key residues (Tyr121 and Tyr70) and **1a** in the PAS were revealed by the high H-bond occupancy rates (92.82% and 60.46%). In the case of **5e**/AChE complex, there were three conserved H-bonds formed between AChE and **5e** with a particularly strong one (99.74%) arising from key residue Gly199 in the CAS. As shown in Table 3, **5e** also had more hydrophobic interactions with AChE than **1a**. Therefore, it was proposed that **5e** could have more potent binding affinity than **1a** based on the H-bond and hydrophobic analyses, which were in good agreement with the experimental results that **5e** displayed better inhibitory activity against AChE than **1a**. Then MM-PBSA calculation was performed to obtain the free binding energy, and the results were shown in Table 4. Taken together, it was confirmed that **5e** did have more potent binding affinity with AChE than **1a**.

2.6. Prediction of pharmacokinetic properties

From the data in Table 5, the MW (< 500 Da) and PSA-2D value (< 108 $Å^2$) of each compound fell into the range of marketed CNS drugs [14,30]. Also, most of them such as **5a–5f** were predicted to have high lipophilicity, acceptable solubility and absorption level, and **5a–5c**

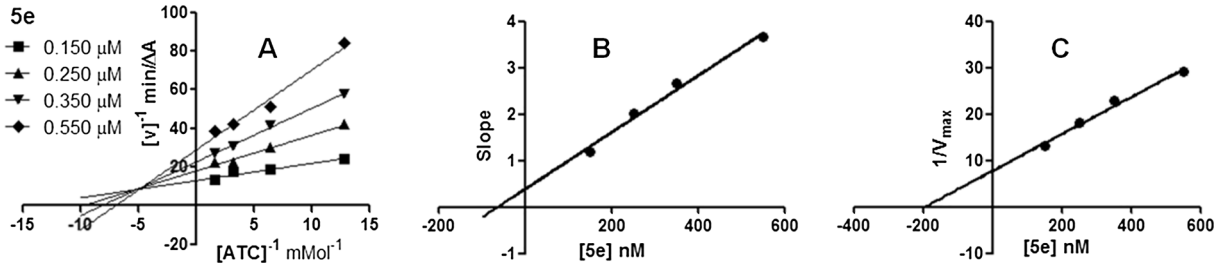

Fig. 4. Kinetic assay on AChE inhibition displayed by **5e**. (A) Lineweaver-Burk reciprocal plots of initial velocity and increasing substrate concentrations (0.078–0.625 mM); (B) Secondary plot of slopes versus **5e** concentrations; (C) Secondary plot of $1/V_{max}$ versus **5e** concentrations.

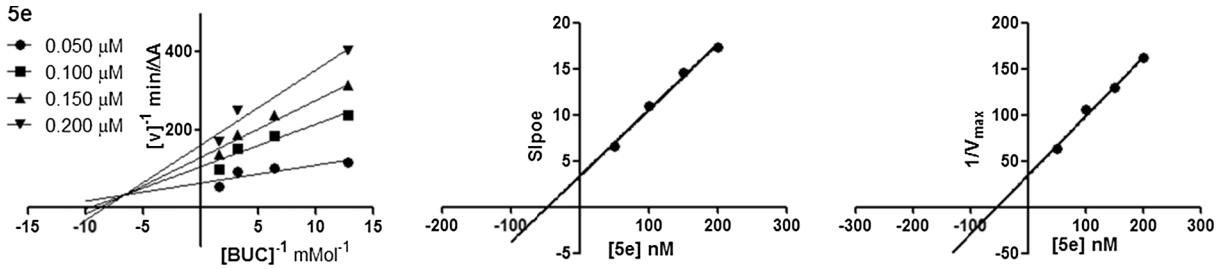

Fig. 5. Kinetic assay on BChE inhibition displayed by **5e**. (A) Lineweaver-Burk reciprocal plots of initial velocity and increasing substrate concentrations (0.078–0.625 mM); (B) Secondary plot of slopes versus **5e** concentrations; (C) Secondary plot of $1/V_{max}$ versus **5e** concentrations.

displayed moderate BBB penetration level. Importantly, all of them may not bind to PPB and CYP2D6, which possibly indicated fewer side effects of this series of compounds.

2.7. Effect on mouse brain neural network electrical activity study

Synchronized oscillatory activity of the brain represents a core mechanism for communications within cortical and subcortical networks [31], and the progression of AD is associated with abnormal network rhythmic activities in the brain [32]. Suppression of long-term fluctuations and enhancement of the frequency of the neural electrical activity have been shown to increase the ability of neurons to respond to external information [33]. In addition, cognition-enhancing drugs elicit similar modulation on network activities [34]. To test the potential effects of **5e** on neural network activity, we generated *in vitro* mouse brain neural network using primary hippocampal neurons (Fig. 10A). Co-cultured neuron/glia cells *in vitro* develop both inhibitory and excitatory connections and elicit oscillatory activities (synchronized periodic bursting) [35]. To monitor the network activity, we infected the cultures with lentivirus that specifically expressed GCaMP6 in neurons under a human synapsin I promoter. GCaMP6 is an ultrasensitive calcium indicator that can get brighter when binding with calcium [36]. Since the firing activity of a neuron is accompanied by calcium influx, GCaMP6 can thus be used to report the firing activity of the neurons. As a result, the cultured neural network will blink under fluorescent microscope during synchronized network oscillation (Fig. 10B and D).

We first tested the effect of **5e** on the network activity. After a stable baseline recording of 1 h, 50 nM **5e** was added into the medium and the recording continued for another 2 h. **5e** caused significant increase in the frequency ($n = 6$; $p < 0.05$; paired *t*-test), a dramatic decrease in the duration of each burst, and a moderate decrease in the overall activity of the network quantified by the average GCaMP6 intensity during the recording (Fig. 10B and C). Nevertheless, **5e** induced mixed changes in the peak of the burst firing (Fig. 10C). Similar effects can be induced using tacrine ($n = 6$), but with a much higher concentration (1 μM, Fig. 10D and E). These results indicate that **5e** exhibits similar effects to tacrine in modulating network activity, but most likely with much stronger efficacy.

3. Conclusion

In summary, a series of novel IAA-tarcine hybrids were prepared based on the analysis of binding mode of lead **1a** with AChE, and their dual AChE/BChE inhibitory activities were then evaluated. Several hybrids, e.g., **5d** and **5e**, displayed potent dual activities against AChE/BChE with IC_{50} values at low nanomolar level. The preliminary SAR analysis indicated that the optimal distance for a diamino linker between IAA and tacrine should be a 6-carbon chain length in AChE bioassay. In addition, **5e** exhibits much stronger effect in modulating neural network activity compared to tacrine, indicating better anti-dementia and nootropic potentials. In the present study, the biological evaluation together with computational analyses demonstrate that these IAA-tacrine hybrids may serve as a new template for developing multifunctional anti-AD drugs. Further structural modifications to improve drug-like properties are in progress and will be reported in due course.

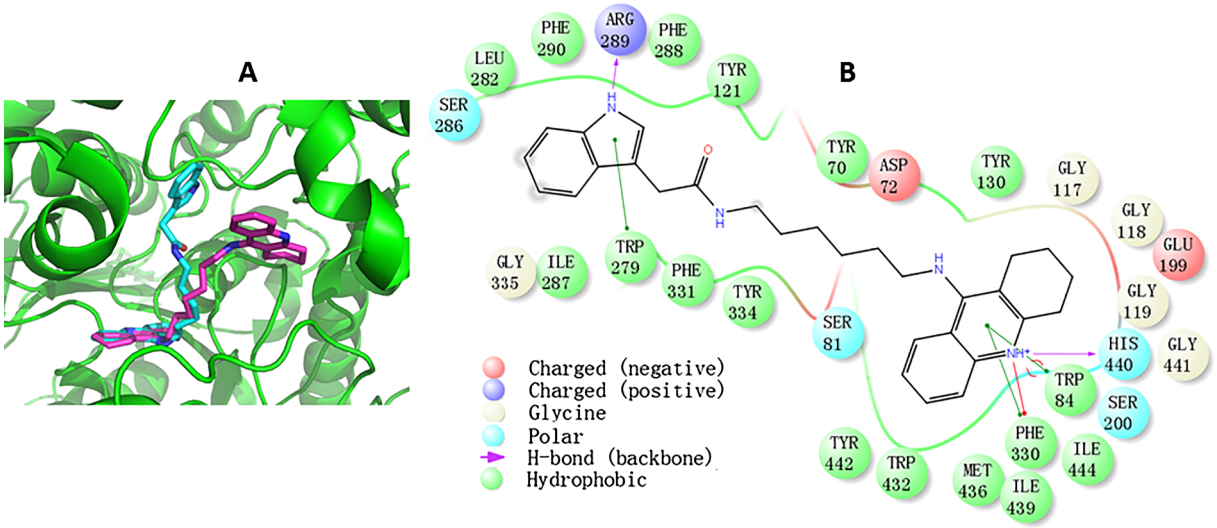

Fig. 6. (A) The proposed orientation of **5e** (carbon in blue) in the active of AChE (PDB: 5EI5) with **AA7** in purple color; (B) The binding mode of **5e** in the active site of AChE.

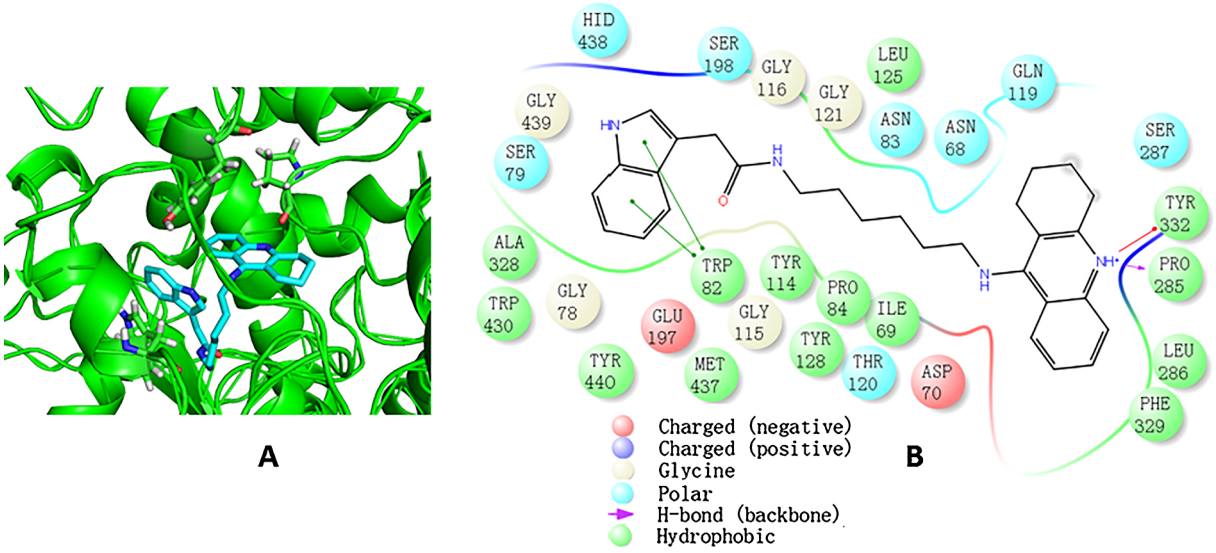

Fig. 7. (A) The proposed orientation of **5e** (carbon in blue) in the active of BChE (PDB: 4BDS) active site; (B) The binding mode of **5e** in the active site of BChE.

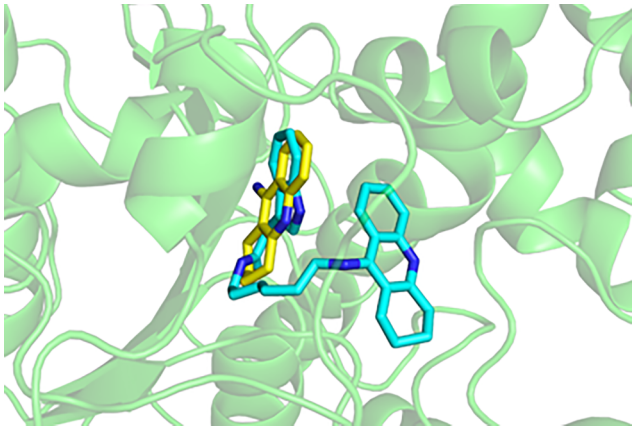

Fig. 8. The binding modes of **5e** (carbon in blue) and tacrine (carbon in yellow) generated by molecular docking.

Table 3
Residues involved in hydrophobic interactions (occupancies > 50%) with the inhibitors during the simulation time and the corresponding occupancy rates.

Residues	1a	5e
Tyr70	96%	72%
Asp72	86%	3%
Trp84	89%	100%
Tyr121	90%	90%
Ser122	55%	83%
Gly123	0.0%	64%
Glu199	0.0%	67%
Trp279	100%	52%
Phe290	26%	50%
Phe330	36%	95%
Tyr334	94%	93%

Table 4
The binding free energy of AChE to **1a** and **5e**.[a]

Inhibitors	ΔG_{gas}	ΔG_{solv}	ΔG
1a	−222.94	195.84	−27.10
5e	−248.78	200.58	−48.20

[a] All calculated values obtain by MM-PBSA method were given in kcal/mol. ΔG_{gas} represents the binding free energy in vacuum; ΔG_{solv} represents the solvation free energy change; $\Delta G = \Delta G_{gas} + \Delta G_{solv}$.

4. Experimental section

4.1. Chemistry

4.1.1. General methods

Melting points were measured by a Melting Point YRY-3 apparatus (Tianjin Precision Apparatus Factory, China). Commercially available reagents were used without further purification. Organic solvents were

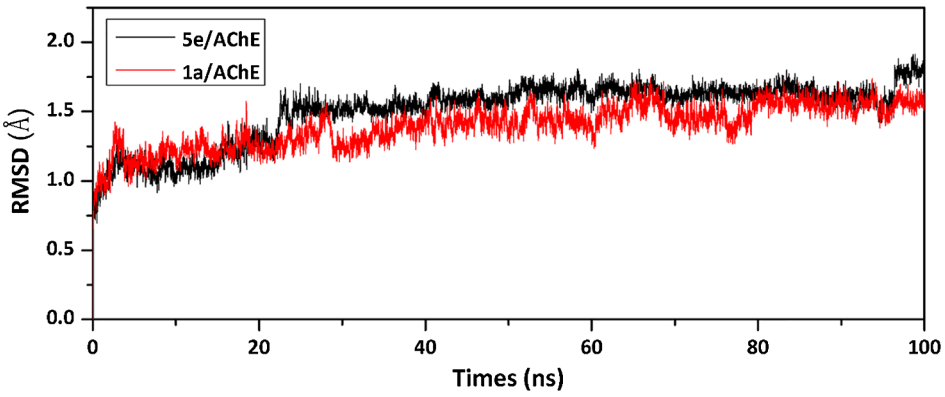

Fig. 9. Time dependencies of RMSDs for the backbone atoms of the **1a**/AChE and **5e**/AChE complexes.

Table 5
Prediction of pharmacokinetic properties of **5a–5g**.

No.	MW	PSA-2D	AlogP98	Solubility level	Absorption level	BBB level	PPB	CYP2D6
5a	398	69.237	4.53	2	0	1	FALSE	FALSE
5b	412	69.237	4.592	2	0	1	FALSE	FALSE
5c	426	69.237	5.172	1	0	1	FALSE	FALSE
5d	440	69.237	5.628	1	1	4	FALSE	FALSE
5e	453	57.976	6.8	1	1	4	FALSE	FALSE
5f	468	69.237	6.541	1	2	4	FALSE	FALSE
5g	481	57.976	7.712	1	3	4	FALSE	FALSE

PSA-2D: Polar surface area; AlogP98: Lipophilicity descriptor; Solubility Level: (0, Good; 1, Moderate; 2, Poor; 3, Very poor); Absorption Level: (0, Good; 1, Moderate; 2, Poor; 3, Very poor); BBB Level: (0, very high blood-brain barrier penetration; 1, high; 2, medium; 3, low; 4, undefined).

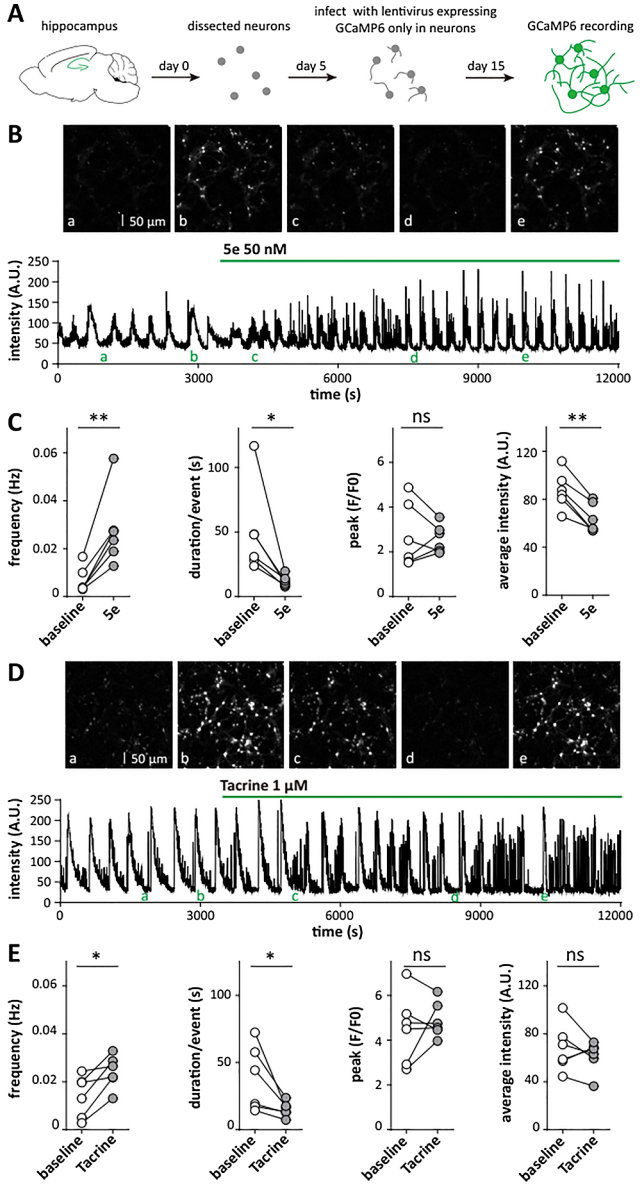

Fig. 10. Influence of **5e** and tacrine on neuronal network activity. (A) Schematic illustration of the experiment. Hippocampal neurons and glia were dissected on day 0 and co-cultured in a dish. Cultures were infected on day 5 using lentivirus and images collected on day 15. (B) Representative time-course plot of the average activity of a neuronal network before and after 50 nM **5e** application. Images of denoted time points are shown on the top of the panel; (C) Quantification of parameters. Each dot represents an averaged result of a neural network. (D) and (E) same to (B) and (C) but showing effects of 1 μM tacrine. $^{**}p < 0.01$, $^{*}p < 0.05$, ns non-significant, paired *t*-test.

evaporated with reduced pressure using a Büchi R-100 evaporator. Reactions were monitored by TLC using Yantai Jingyou (China) GF254 silica gel plates. Silica gel column chromatography was performed on silica gel (200–300 mesh) from Qingdao Hailang (China). The purity of the samples was determined by an analytical Agilent 1260 HPLC with ZDRBAX SB-C18 column (4.6 mm × 150 mm) using parameters as follows: H_2O/MeOH, 20/80 to 0/100 in 15 min, plus 15 min isocratic MeOH, flow rate at 1.0 mL/min, λ = 254 nm. NMR spectra were measured on Bruker Avance III 600 and 400 MHz spectrometers. Chemical shifts were expressed in δ (ppm) and coupling constants (J) in Hz with solvent signals as internal standards ($CDCl_3$, δ_H 7.26 ppm and δ_C 77.0 ppm; CD_3OD, δ_H 3.31 ppm and δ_C 49.0 ppm; DMSO-d_6, δ_H 2.50 ppm and δ_C 39.5 ppm). ESI-MS analyses were performed on an Agilent 1260–6460 Triple Quard LC-MS instrument. HR-ESI-MS data were acquired on an Agilent Q-TOF 6520.

4.1.2. General procedures for the preparation of 1a–1p

The mixtures of IAA (175 mg, 1 mmol), HOBT (153 mg, 1 mmol), EDCI (170 mg, 1.1 mmol), DIEA (260 μL, 1.5 mmol), and the corresponding amines (1.5 mmol) in 5 mL dichloromethane were stirred at room temperature for 12 h. The reaction solvent was removed under reduced pressure, and the obtained residues were purified on silica gel columns eluted with CH_2Cl_2-MeOH to yield compounds **1a–1p**.

*4.1.2.1. N-(2-(Diisopropylamino)ethyl)-2-(1H-indol-3-yl)acetamide (**1a**).* Yellow solid in 92.2% yield, mp 84.0–85.3 °C. HPLC purity: 97.1% yield, t_R = 8.04 min. ^{1}H NMR (600 MHz, CD_3OD) δ 7.48 (d, J = 7.9 Hz, 1H), 7.36 (d, J = 8.1 Hz, 1H), 7.18 (s, 1H), 7.11 (dd, J = 8.1, 7.6 Hz, 1H), 7.02 (dd, J = 7.9, 7.6 Hz, 1H), 3.67 (s, 2H), 3.12 (t, J = 6.7 Hz, 2H), 2.85–2.78 (m, 2H), 2.45 (t, J = 6.7 Hz, 2H), 0.80 (d, J = 7.6 Hz, 12H). ^{13}C NMR (150 MHz, CD_3OD) δ 174.9, 138.3, 128.5, 125.3, 122.8, 120.2, 119.2, 112.5, 108.8, 49.9, 44.4, 40.2, 33.9, 20.6. ESI-MS m/z 302.2 $[M+H]^+$. HR-ESIMS: $[M+H]^+$ calcd for $C_{18}H_{28}N_3O^+$ 302.2227, found 302.2228.

*4.1.2.2. 2-(1H-Indol-3-yl)acetamide (**1b**).* White solid in 25% yield, mp 158.5–160.6 °C. HPLC purity: 98.7% yield, t_R = 9.89 min. ^{1}H NMR (600 MHz, CD_3OD) δ 7.54 (d, J = 7.9 Hz, 1H), 7.35 (d, J = 8.1 Hz, 1H), 7.18 (s, 1H), 7.10 (dd, J = 8.1, 7.5 Hz, 1H), 7.02 (dd, J = 7.9, 7.5 Hz, 1H), 3.65 (s, 2H). ^{13}C NMR (150 MHz, CD_3OD) δ 178.0, 138.1, 128.5, 124.9, 122.5, 119.9, 119.3, 112.2, 109.5, 33.5. ESI-MS m/z 175.4 $[M+H]^+$. HR-ESIMS: $[M+H]^+$ calcd for $C_{10}H_{11}N_2O^+$ 175.0866, found 175.0865.

*4.1.2.3. N-(2-(Dimethylamino)ethyl)-2-(1H-indol-3-yl)acetamide (**1c**).* Yellow solid in 86.5% yield, mp 98.2–100.4 °C. HPLC purity: 98.1% yield, t_R = 5.83 min. ^{1}H NMR (600 MHz, CD_3OD) δ 7.54 (d, J = 8.0 Hz, 1H), 7.37 (d, J = 8.1 Hz, 1H), 7.20 (s, 1H), 7.12 (dd, J = 8.1, 7.0 Hz, 1H), 7.03 (dd, J = 8.0, 7.0 Hz, 1H), 3.68 (s, 2H), 3.32 (t, J = 6.7 Hz, 2H), 2.44 (t, J = 6.7 Hz, 2H), 2.24 (s, 6H). ^{13}C NMR (150 MHz, CD_3OD) δ 175.1, 138.2, 128.5, 125.0, 122.6, 120.0, 119.3, 112.3, 109.3, 59.1, 45.3, 38.0, 34.0. ESI-MS m/z 246.2 $[M+H]^+$. HR-

ESIMS: $[M+H]^+$ calcd for $C_{14}H_{20}N_3O^+$ 246.1601, found 246.1609.

4.1.2.4. N-(2-(Diethylamino)ethyl)-2-(1H-indol-3-yl)acetamide ***(1d)***. Yellow oil in 68.0% yield. HPLC purity: 98.7% yield, t_R = 7.51 min. ^{1}H NMR (600 MHz, CD_3OD) δ 7.51 (d, J = 8.0 Hz, 1H), 7.35 (d, J = 7.5 Hz, 1H), 7.18 (s, 1H), 7.11 (dd, J = 7.5, 7.0 Hz, 1H), 7.02 (dd, J = 8.0, 7.0 Hz, 1H), 3.66 (s, 2H), 3.24 (t, J = 6.7 Hz, 2H), 2.48 (t, J = 6.7 Hz, 2H), 2.44 (q, J = 7.2 Hz, 4H), 0.89 (t, J = 7.2 Hz 6H). ^{13}C NMR (150 MHz, CD_3OD) δ 174.9, 138.2, 128.5, 125.1, 122.6, 120.0, 119.3, 112.4, 109.1, 52.2, 47.9, 37.8, 33.9, 11.6. ESI-MS *m/z* 274.7 $[M+H]^+$. HR-ESIMS: $[M+H]^+$ calcd for $C_{16}H_{24}N_3O^+$ 274.1914, found 274.1915.

4.1.2.5. N-(2-(Ethylamino)ethyl)-2-(1H-indol-3-yl)acetamide ***(1e)***. Yellow oil in 82.6% yield. HPLC purity: 95.5% yield, t_R = 14.64 min. ^{1}H NMR (600 MHz, $CDCl_3$) δ 8.41 (brs, 1H, NH), 7.30 (d, J = 8.1 Hz, 1H), 7.25 (d, J = 8.1 Hz, 1H), 7.12 (dd, J = 8.1, 5.4 Hz, 1H), 7.10 (dd, J = 8.1, 5.4 Hz, 1H), 6.65 (s, 1H), 6.44 (t, J = 4.5 Hz, 1H), 3.57 (s, 2H), 3.38 (t, J = 5.3 Hz, 2H), 3.40–3.36 (m, 2H), 3.17 (q, J = 7.1 Hz, 2H), 1.05 (t, J = 7.1 Hz, 3H). ^{13}C NMR (150 MHz, $CDCl_3$) δ 172.4, 136.5, 127.2, 124.2, 122.7, 119.7, 118.8, 111.6, 109.1, 53.6, 44.2, 39.2, 33.4, 14.2. ESI-MS *m/z* 246.1 $[M+H]^+$. HR-ESIMS: $[M+H]^+$ calcd for $C_{14}H_{20}N_3O^+$ 246.1601, found 246.1611.

4.1.2.6. Tert-butyl (2-(2-(1H-indol-3-yl)acetamido)ethyl)carbamate ***(1f)***. White solid in 95.2% yield, mp 138.5–141.2 °C. HPLC purity: 96.1% yield, t_R = 14.36 min. ^{1}H NMR (600 MHz, CD_3OD) δ 7.52 (d, J = 7.9 Hz, 1H), 7.35 (d, J = 8.1 Hz, 1H), 7.17 (s, 1H), 7.10 (dd, J = 8.1, 7.2 Hz, 1H), 7.02 (dd, J = 7.9, 7.2 Hz, 1H), 3.65 (s, 2H), 3.23 (t, J = 6.1 Hz, 2H), 3.10 (t, J = 6.1 Hz, 2H), 1.40 (s, 9H). ^{13}C NMR (150 MHz, CD_3OD) δ 175.3, 158.5, 138.2, 128.5, 125.0, 122.6, 119.8, 119.3, 112.4, 109.2, 80.1, 40.9, 40.6, 34.0, 28.4. ESI-MS *m/z* 340.1 $[M+Na]^+$. HR-ESIMS: $[M+Na]^+$ calcd for $C_{17}H_{23}N_3NaO_3^+$ 340.1632, found 340.1633.

4.1.2.7. 2-(1H-indol-3-yl)-N-(2-(pyrrolidin-1-yl)ethyl)acetamide ***(1g)***. White solid in 86.2% yield, mp 106.5–107.4 °C. HPLC purity: 98.6% yield, t_R = 8.66 min. ^{1}H NMR (600 MHz, $CDCl_3$) δ 8.83 (brs, 1H, NH), 7.55 (d, J = 7.9 Hz, 1H), 7.36 (d, J = 8.1 Hz, 1H), 7.20 (dd, J = 8.1, 7.2 Hz, 1H), 7.12 (dd, J = 7.9, 7.1 Hz, 1H), 6.97 (d, J = 2.1 Hz, 1H), 6.28 (s, 1H), 3.70 (s, 2H), 3.34–3.29 (m, 2H), 2.49 (t, J = 6.2 Hz, 2H), 2.37–2.32 (m, 4H), 1.62–1.55 (m, 4H). ^{13}C NMR (150 MHz, $CDCl_3$) δ 171.9, 136.6, 127.2, 123.9, 122.4, 119.8, 118.8, 111.5, 109.0, 54.4, 53.8, 38.3, 33.6, 23.5. ESI-MS *m/z* 272.2 $[M+H]^+$. HR-ESIMS: $[M+H]^+$ calcd for $C_{16}H_{22}N_3O^+$ 272.1757, found 272.1755.

4.1.2.8. 1. 2-(1H-Indol-3-yl)-N-(2-morpholinoethyl)acetamide ***(1h)***. Yellow solid in 83.0% yield, mp 108.5–110.4 °C. HPLC purity: 97.1% yield, t_R = 6.56 min. ^{1}H NMR (600 MHz, CD_3OD) δ 7.51 (d, J = 7.9 Hz, 1H), 7.37 (d, J = 8.2 Hz, 1H), 7.21 (s, 1H), 7.12 (dd, J = 8.2, 7.4 Hz, 1H), 7.02 (dd, J = 7.9, 7.4 Hz, 1H), 3.67 (s, 2H), 3.43–3.37 (m, 4H), 3.26 (t, J = 6.3 Hz, 2H), 2.35 (t, J = 6.3 Hz, 2H), 2.28–2.22 (m, 4H). ^{13}C NMR (150 MHz, CD_3OD) δ 174.8, 138.3, 128.5, 125.3, 122.7, 120.1, 119.3, 112.5, 109.2, 67.7, 57.8, 54.2, 37.0, 34.0. ESI-MS *m/z* 288.2 $[M+H]^+$. HR-ESIMS: $[M+H]^+$ calcd for $C_{16}H_{22}N_3O_2^+$ 288.1707, found 288.1704.

4.1.2.9. N-(2,2-Dimethoxyethyl)-2-(1H-indol-3-yl)acetamide ***(1i)***. White solid in 59.8% yield, mp 58.5–60.0 °C. HPLC purity: 97.2% yield, t_R = 12.13 min. ^{1}H NMR (600 MHz, $CDCl_3$) δ 8.39 (brs, 1H, NH), 7.55 (d, J = 7.9 Hz, 1H), 7.39 (d, J = 8.2 Hz, 1H), 7.22 (dd, J = 8.2, 7.0 Hz, 1H), 7.14 (dd, J = 7.9, 7.0 Hz, 1H), 7.12 (s, 1H), 5.88 (brs, 1H, NH), 4.26 (t, J = 5.5 Hz, 1H), 3.74 (s, 2H), 3.33 (dd, J = 5.8, 5.5 Hz, 2H), 3.24 (s, 6H). ^{13}C NMR (150 MHz, $CDCl_3$) δ 171.8, 136.5, 127.0, 123.9, 122.7, 120.1, 118.9, 111.5, 109.0, 102.9, 54.6, 41.2, 33.6. ESI-MS *m/z* 285.1 $[M+Na]^+$. HR-ESIMS: $[M+Na]^+$ calcd for $C_{14}H_{18}N_2NaO_3^+$ 285.1210, found 285.1216.

4.1.2.10. N-(2,2-Diethoxyethyl)-2-(1H-indol-3-yl)acetamide ***(1j)***. Yellow oil in 40.4% yield. HPLC purity: 95.7% yield, t_R = 13.97 min. ^{1}H NMR (600 MHz, $CDCl_3$) δ 8.37 (brs, 1H), 7.55 (d, J = 7.9 Hz, 1H), 7.39 (d, J = 8.1 Hz, 1H), 7.22 (dd, J = 8.1, 7.4 Hz, 1H), 7.14 (dd, J = 7.9, 7.4 Hz, 1H), 7.12 (s, 1H), 5.91 (brs, 1H, NH), 4.35 (t, J = 5.6 Hz, 1H), 3.74 (s, 2H), 3.58–3.52 (m, 2H), 3.33 (q, J = 7.0 Hz, 4H), 0.99 (t, J = 7.0 Hz, 6H). ^{13}C NMR (150 MHz, $CDCl_3$) δ 171.7, 136.6, 127.1, 123.8, 122.8, 120.2, 118.8, 111.5, 109.1, 101.0, 63.1, 42.1, 33.5, 15.2. ESI-MS *m/z* 313.1 $[M+Na]^+$. HR-ESIMS: $[M+Na]^+$ calcd for $C_{16}H_{22}N_2NaO_3^+$ 313.1523, found 313.1527.

4.1.2.11. 2-(1H-Indol-3-yl)-N-(2-(methylsulfonyl)ethyl)acetamide ***(1k)***. Yellow oil in 54.2% yield. HPLC purity: 95.4% yield, t_R = 10.24 min. ^{1}H NMR (600 MHz, CD_3OD) δ 7.53 (d, J = 7.9 Hz, 1H), 7.35 (d, J = 8.2 Hz, 1H), 7.18 (s, 1H), 7.11 (dd, J = 8.2, 7.0 Hz, 1H), 7.02 (dd, J = 7.9, 7.0 Hz, 1H), 3.66 (s, 2H), 3.60 (t, J = 6.6 Hz, 2H), 3.20 (t, J = 6.6 Hz, 2H), 2.79 (s, 3H). ^{13}C NMR (150 MHz, CD_3OD) δ 175.3, 138.1, 128.5, 125.1, 122.7, 120.1, 119.3, 112.4, 109.0, 54.3, 41.1, 34.6, 33.9. ESI-MS *m/z* 303.0 $[M+Na]^+$. HR-ESIMS: $[M+H]^+$ calcd for $C_{13}H_{17}N_2O_3S^+$ 281.0954, found 281.0960.

4.1.2.12. Methyl 5-(2-(1H-indol-3-yl)acetamido)pentanoate ***(1l)***. Colorless oil in 50.8% yield. HPLC purity: 96.2% yield, t_R = 13.20 min. ^{1}H NMR (600 MHz, $CDCl_3$) δ 8.75 (brs, 1H, NH), 7.54 (d, J = 7.9 Hz, 1H), 7.40 (d, J = 8.2 Hz, 1H), 7.22 (dd, J = 8.2, 7.1 Hz, 1H), 7.13 (dd, J = 7.9, 7.1 Hz, 1H), 7.11 (d, J = 2.3 Hz, 1H), 5.81 (brs, 1H, NH), 3.73 (s, 2H), 3.62 (s, 3H), 3.21–3.14 (m, 2H), 2.24 (t, J = 7.4 Hz, 2H), 1.53–1.47 (m, 2H), 1.43–1,36 (m, 2H). ^{13}C NMR (150 MHz, $CDCl_3$) δ 174.0, 171.8, 136.6, 127.1, 124.0, 122.6, 120.1, 118.7, 111.6, 108.8, 51.6, 39.1, 33.5, 29.0, 22.1. ESI-MS *m/z* 289.1 $[M+H]^+$. HR-ESIMS: $[M+H]^+$ calcd for $C_{16}H_{21}N_2O_3^+$ 289.1547, found 289.1540.

4.1.2.13. Tert-butyl (5-(2-(1H-indol-3-yl)acetamido)pentyl)carbamate ***(1m)***. Yellow oil in 69.6% yield. HPLC purity: 97.4%, t_R = 15.37 min. ^{1}H NMR (600 MHz, $CDCl_3$) δ 9.00 (s, 1H), 7.52 (d, J = 7.8 Hz, 1H), 7.39 (d, J = 8.0 Hz, 1H), 7.21 (dd, J = 8.0, 7.4 Hz, 1H), 7.12 (dd, J = 7.8, 7.4 Hz, 1H), 7.10 (d, J = 2.3 Hz, 1H), 5.80 (t, J = 5.7 Hz, 1H, NH), 4.57 (brs, 1H, NH), 3.72 (s, 2H), 3.17–3.11 (m, 2H), 3.03–2.92 (m, 2H), 1.44 (s, 9H), 1.37–1.30 (m, 4H), 1.16–1.09 (m, 2H). ^{13}C NMR (150 MHz, $CDCl_3$) δ 171.8, 156.2, 136.6, 127.1, 124.1, 122.5, 119.9, 118.7, 111.7, 108.8, 79.2, 40.4, 39.3, 33.5, 29.6, 29.1, 28.5, 23.9. ESI-MS *m/z* 394.1 $[M+Cl]^-$. HR-ESIMS: $[M+Na]^+$ calcd for $C_{20}H_{29}N_3NaO_3^+$ 382.2101, found 382.2100.

4.1.2.14. 5-(2-(1H-indol-3-yl)acetamido)-N-(2-(diisopropylamino)ethyl) pentanamide ***(1n)***. Colorless oil in 71.4% yield. HPLC purity: 99.0%, t_R = 8.25 min. ^{1}H NMR (600 MHz, $CDCl_3$) δ 9.19 (brs, 1H, NH), 7.51 (d, J = 7.7 Hz, 1H), 7.37 (d, J = 8.3 Hz, 1H), 7.18 (dd, J = 7.7, 7.3 Hz, 1H), 7.09 (dd, J = 8.3, 7.3 Hz, 1H), 7.07 (d, J = 2.3 Hz, 1H), 6.24 (brs, 1H, NH), 5.94 (t, J = 5.7 Hz, 1H, NH), 3.69 (s, 2H), 3.20–3.16 (m, 2H), 3.14 (q, J = 6.7 Hz, 2H), 3.02–2.96(m, 2H), 2.54 (t, J = 6.1 Hz, 2H), 2.09 (t, J = 7.5 Hz, 2H), 1.54–1.47 (m, 2H), 1.41–1.34 (m, 2H), 0.99 (d, J = 6.7 Hz, 12H). ^{13}C NMR (150 MHz, $CDCl_3$) δ 172.7, 171.9, 136.6, 127.1, 124.1, 122.3, 119.8, 118.6, 111.6, 108.6, 57.0, 45.6, 39.1, 38.2, 36.0, 33.5, 29.0, 22.8, 20.7. ESI-MS *m/z* 401.3 $[M+H]^+$. HR-ESIMS: $[M+H]^+$ calcd for $C_{23}H_{37}N_4O_2^+$ 401.2911, found 401.2914.

4.1.2.15. 5-(2-(1H-indol-3-yl)acetamido)-N-(2,2-dimethoxyethyl) pentanamide ***(1o)***. Yellow oil in 92.4% yield. HPLC purity: 98.2%, t_R = 12.09 min. ^{1}H NMR (600 MHz, $CDCl_3$) δ 9.02 (brs, 1H, NH), 7.52 (d, J = 7.9 Hz, 1H), 7.37 (d, J = 8.2 Hz, 1H), 7.19 (dd, J = 8.2, 7.1 Hz, 1H), 7.11 (dd, J = 7.9, 7.1 Hz, 1H), 7.08 (d, J = 2.3 Hz, 1H), 5.92 (t, J = 5.6 Hz, 1H, NH), 5.87 (t, J = 5.6 Hz, 1H, NH), 4.34 (t, J = 5.2 Hz, 1H,), 3.70 (s, 2H), 3.37–3.33 (m, 8H), 3.17–3.12 (m, 2H), 2.09 (t, J = 7.5 Hz, 2H), 1.52–1.46 (m, 2H), 1.40–1.34 (m, 2H). ^{13}C NMR (150 MHz, $CDCl_3$) δ 173.1, 171.9, 136.6, 127.1, 124.1, 122.5, 119.9,

118.7, 111.6, 108.7, 102.6, 54.4, 40.9, 38.9, 35.8, 33.5, 28.9, 22.7. ESI-MS *m/z* 396.1 $[M + Cl]^-$. HR-ESIMS: $[M+Na]^+$ calcd for $C_{19}H_{27}N_3NaO_4^+$ 384.1894, found 384.1883.

*4.1.2.16. 5-(2-(1H-indol-3-yl)acetamido)-N-(2,2-diethoxyethyl) pentanamide (**1q**).* Colorless oil in 62.3% yield. HPLC purity: 99.4%, t_R = 13.71 min. ^{1}H NMR (600 MHz, $CDCl_3$) δ 9.08 (brs, 1H, NH), 7.51 (d, *J* = 8.3 Hz, 1H), 7.37 (d, *J* = 8.1 Hz, 1H), 7.19 (dd, *J* = 8.1, 7.2 Hz, 1H), 7.10 (dd, *J* = 8.3, 7.1 Hz, 1H), 7.07 (d, *J* = 2.3 Hz, 1H), 5.93 (t, *J* = 5.8 Hz, 1H, NH), 5.87 (t, *J* = 5.5 Hz, 1H, NH), 4.47 (t, *J* = 5.2 Hz, 1H), 3.71–3.65 (m, 4H), 3.54–3.48 (m, 2H), 3.34 (t, *J* = 5.5 Hz, 2H), 3.14 (q, *J* = 7.1 Hz,2H), 2.08 (t, *J* = 7.5 Hz, 2H), 1.52–1.45 (m, 2H), 1.40–1.33 (m, 2H), 1.19 (t, *J* = 7.1 Hz, 6H). ^{13}C NMR (150 MHz, $CDCl_3$) δ 173.1, 172.0, 136.6, 127.1, 124.1, 122.4, 119.9, 118.6, 111.6, 108.7, 100.8, 62.9, 41.9, 38.9, 35.8, 33.5, 28.9, 22.7, 15.4. ESI-MS *m/z* 390.1 $[M+H]^+$. HR-ESIMS: $[M+Na]^+$ calcd for $C_{21}H_{31}N_3NaO_4^+$ 412.2207, found 412.2210.

*4.1.3. 2-Aminobenzoic acid (**2**)*

2-Nitrobenzoic acid (3.006 g, 18 mmol) and Pd/C (954 mg, 9 mmol) were added into 20 mL methanol under hydrogen, and the mixture was stirred at room temperature for 12 h. The solution was filtered to remove the catalyst, and then the filtrate was concentrated under reduced pressure to give 2-aminobenzoic acid **2**. This compound was used in next step without further purification.

*4.1.4. 9-Chloro-1,2,3,4-tetrahydroacridine(**3**)*

Cyclohexanone (1.88 g, 19.2 mmol) was added to a solution of compound **2** (2.20 g, 16 mmol) in 15 mL phosphorus oxychloride. The reaction mixture was stirred at 100 °C for 4 h, and then diluted in ethyl acetate, washed with potassium carbonate solution. The organic phase was dried over sodium sulphate. The product 9-chloroacridine (**3**) was purified by flash column chromatography using mixtures of petroleum ether-acetone. Yellow solid in 61.0% yield, mp 121.8–122.6 °C. ^{1}H NMR (600 MHz, $CDCl_3$) δ 8.16 (d, *J* = 8.3 Hz, 1H), 7.97 (d, *J* = 8.4 Hz, 1H), 7.66 (dd, *J* = 8.3, 7.4 Hz, 1H), 7.53 (dd, *J* = 8.4, 7.4 Hz, 1H), 3.13 (t, *J* = 5.6 Hz, 2H), 3.02 (t, *J* = 6.4 Hz, 2H), 1.98–1.91 (m, 4H). ^{13}C NMR (150 MHz, $CDCl_3$) δ 159.7, 146.8, 141.6, 129.4, 129.0, 128.8, 126.6, 125.5, 123.8, 34.4, 27.7, 22.8, 22.8. ESI-MS *m/z* 218.2 $[M+H]^+$.

*4.1.5. General procedures for the preparation of **4a–4g***

To a solutions of **3** (235 mg, 2 mmol) in 5 mL pentanol were added the corresponding diamines (6 mmol). The reaction mixtures were stirred at 140 °C overnight. After cooling to room temperature, the residues were purified on silica gel columns using CH_2Cl_2-CH_3OH with 0.5% Et_3N to give the corresponding intermediates **4a–4g**.

*4.1.5.1. N^1-(1,2,3,4-Tetrahydroacridin-9-yl)ethane-1,2-diamine (**4a**).* Brown oil in 33% yield. ^{1}H NMR (600 MHz, $CDCl_3$) δ 8.03 (d, *J* = 9.1 Hz, 2H), 8.01 (d, *J* = 9.8 Hz, 2H), 7.56 (dd, *J* = 9.8, 7.0 Hz, 1H), 7.35 (dd, *J* = 9.1, 7.0 Hz, 1H), 3.57 (t, *J* = 5.8 Hz, 2H), 3.10 (brs, 2H), 2.98 (t, *J* = 5.8 Hz,2H), 2.74 (brs, 2H), 1.95–1.86 (m, 4H). ^{13}C NMR (150 MHz, $CDCl_3$) δ 157.4, 151.8, 146.2, 129.1, 127.5, 123.9, 123.2, 119.7, 115.7, 50.6, 42.3, 33.2, 24.7, 23.0, 22.6. ESI-MS *m/z* 242.6 $[M+H]^+$.

*4.1.5.2. N^1-(1,2,3,4-Tetrahydroacridin-9-yl)propane-1,3-diamine (**4b**).* Brown oil in 68.2% yield. ^{1}H NMR (600 MHz, CD_3OD) δ 8.07 (d, *J* = 8.6 Hz, 1H), 7.71 (t, *J* = 6.9 Hz, 1H), 7.68 (dd, *J* = 8.3, 6.9 Hz, 1H), 7.40 (dd, *J* = 8.6, 8.3 Hz, 1H), 3.93 (t, *J* = 6.0 Hz, 2H), 2.75 (brs, 2H), 2.41 (brs, 2H), 1.97 (t, *J* = 6.0 Hz, 2H), 1.81–1.71 (m, 6H). ^{13}C NMR (150 MHz, CD_3OD) δ 156.7, 153.2, 141.7, 132.9, 134.2, 126.1, 125.6, 120.2, 117.4, 52.8, 45.9, 32.6, 30.3, 25.0, 22.9, 22.1. ESI-MS *m/z* 256.2 $[M+H]^+$.

*4.1.5.3. N^1-(1,2,3,4-Tetrahydroacridin-9-yl)butane-1,4-diamine (**4c**).* Brown oil in 21.6% yield. ^{1}H NMR (600 MHz, $CDCl_3$) δ 7.98 (d, *J* = 8.5 Hz, 2H), 7.96 (d, *J* = 8.5 Hz, 1H), 7.58 (dd, *J* = 8.5, 7.0 Hz, 1H), 7.37 (dd, *J* = 8.5, 7.0 Hz, 1H), 3.62 (t, *J* = 7.1 Hz, 2H), 3.05 (brs, 2H), 2.77 (t, *J* = 7.0 Hz, 2H), 2.67 (brs, 2H), 1.93–1.87 (m, 4H), 1.77–1.71 (m, 2H), 1.63–1.56 (m, 2H). ^{13}C NMR (150 MHz, $CDCl_3$) δ 157.2, 152.2, 145.5, 129.6, 126.4, 124.2, 123.2, 119.2, 114.9, 49.2, 41.4, 32.3, 30.2, 29.1, 24.7, 22.8, 22.3. ESI-MS *m/z* 270.2 $[M+H]^+$.

*4.1.5.4. N^1-(1,2,3,4-Tetrahydroacridin-9-yl)pentane-1,5-diamine (**4d**).* Brown oil in 76.3% yield. ^{1}H NMR (600 MHz, $CDCl_3$) δ 7.94 (d, *J* = 8.4 Hz, 1H), 7.90 (d, *J* = 8.5 Hz, 1H), 7.54 (dd, *J* = 8.5, 7.0 Hz, 1H), 7.34 (dd, *J* = 8.4, 7.0 Hz, 1H), 3.49 (t, *J* = 7.2 Hz, 2H), 3.06 (brs, 2H), 2.70 (brs, 2H), 2.69 (t, *J* = 7.7, 2H), 1.93–1.89 (m, 4H), 1.70–1.64 (m, 2H), 1.51–1.45 (m, 2H), 1.45–1.40 (m, 2H). ^{13}C NMR (150 MHz, $CDCl_3$) δ 158.5, 150.9, 147.5, 128.8, 128.5, 123.8, 122.9, 120.3, 116.0, 49.6, 42.1, 34.1, 31.8, 24.9, 24.4, 23.2, 23.2, 22.9. ESI-MS *m/z* 284.2 $[M+H]^+$.

*4.1.5.5. N^1-(1,2,3,4-Tetrahydroacridin-9-yl)hexane-1,6-diamine (**4e**).* Brown oil in 76.4% yield. ^{1}H NMR (600 MHz, $CDCl_3$) δ 7.95 (d, *J* = 8.4 Hz, 1H), 7.91 (d, *J* = 8.5 Hz, 1H), 7.55 (dd, *J* = 8.5, 7.9 Hz, 1H), 7.34 (dd, *J* = 8.4, 7.9 Hz, 1H), 3.49 (t, *J* = 7.2 Hz, 2H), 3.06 (brs, 2H), 2.70 (brs, 2H), 2.68 (t, *J* = 7.0 Hz, 2H), 1.95–1.88 (m, 4H), 1.71–1.60 (m, 2H), 1.48–1.43 (m, 2H), 1.43–1.38 (m, 2H), 1.38–1.33 (m, 2H). ^{13}C NMR (150 MHz, $CDCl_3$) δ 158.4, 151.0, 147.3, 128.6, 128.5, 123.8, 123.0, 120.2, 115.9, 49.6, 42.1, 34.0, 33.4, 31.9, 26.9, 26.8, 24.9, 23.2, 22.9. ESI-MS *m/z* 298.2 $[M+H]^+$.

*4.1.5.6. N^1-(1,2,3,4-Tetrahydroacridin-9-yl)heptane-1,7-diamine (**4f**).* Brown oil in 69.1% yield. ^{1}H NMR (600 MHz, $CDCl_3$) δ 7.94 (d, *J* = 8.5 Hz, 1H), 7.89 (d, *J* = 8.4 Hz, 1H), 7.53 (dd, *J* = 8.4, 7.3 Hz, 1H), 7.33 (dd, *J* = 8.5, 7.3 Hz, 1H), 3.47 (t, *J* = 7.2 Hz, 2H), 3.05 (brs, 2H), 2.69 (brs, 2H), 2.65 (t, *J* = 7.0 Hz, 2H), 1.92–1.88 (m, 4H), 1.67–1.61 (m, 2H), 1.44–1.40 (m, 2H), 1.39–1.35 (m, 2H), 1.33–1.28 (m, 4H). ^{13}C NMR (150 MHz, $CDCl_3$) δ 158.5, 151.0, 147.5, 128.7, 128.4, 123.7, 123.0, 120.1, 115.9, 49.6, 42.1, 34.0, 33.5, 31.8, 29.3, 27.0, 26.9, 24.9, 23.1, 22.9. ESI-MS *m/z* 312.2 $[M+H]^+$.

*4.1.5.7. N^1-(1,2,3,4-Tetrahydroacridin-9-yl)octane-1,8-diamine (**4g**).* Brown oil in 49.1% yield. ^{1}H NMR (600 MHz, $CDCl_3$) δ 7.95 (d, *J* = 8.4 Hz, 1H), 7.90 (d, *J* = 8.4 Hz, 1H), 7.54 (dd, *J* = 8.4, 7.7 Hz, 1H), 7.33 (dd, *J* = 8.4, 7.7 Hz, 1H), 3.47 (t, *J* = 7.3 Hz, 2H), 3.05 (brs, 2H), 2.70 (brs, 2H), 2.65 (t, *J* = 7.1 Hz, 2H), 1.93–1.87 (m, 4H), 1.68–1.61 (m, 2H), 1.46–1.4 (m, 4H), 1.32–1.26 (m, 6H). ^{13}C NMR (150 MHz, $CDCl_3$) δ 158.5, 151.0, 147.5, 128.7, 128.4, 123.7, 123.0, 120.3, 115.9, 49.6, 42.2, 34.1, 33.7, 31.9, 29.5, 29.4, 27.0, 26.9, 24.9, 23.2, 22.9. ESI-MS *m/z* 326.2 $[M+H]^+$.

*4.1.6. General procedures for the preparation of **5a–5g***

To the mixtures of corresponding diamines **4a–4g** (1 mmol) in 5 mL dichloromethane, IAA (175 mg, 1 mmol), HATU (304 mg, 1.1 mmol), and DIEA (139 μL, 1.5 mmol) were added. The reaction mixtures were stirred at room temperature for 12 h and then concentrated under reduced pressure. The obtained residues were purified on silica gel columns eluted with CH_2Cl_2-CH_3OH with 0.5% Et_3N to give target compounds **5a–5g**.

*4.1.6.1. 2-(1H-Indol-3-yl)-N-(2-((1,2,3,4-tetrahydroacridin-9-yl)amino) ethyl)acetamide (**5a**).* White solid in 43.3% yield, mp 202.1–203.5 °C. HPLC purity: 98.8%, t_R = 12.20 min. ^{1}H NMR (400 MHz, DMSO-d_6) δ 10.96 (brs, 1H, NH), 8.58 (t, *J* = 5.7 Hz, 1H, NH), 8.41 (d, *J* = 8.7 Hz, 1H), 7.97 (d, *J* = 8.1 Hz, 1H), 7.81 (dd, *J* = 8.1, 7.4 Hz, 1H), 7.49 (dd, *J* = 8.7, 7.4 Hz, 1H), 7.41 (d, *J* = 7.9 Hz, 1H), 7.30 (d, *J* = 8.1 Hz, 1H), 7.16 (brs, 1H), 6.98 (dd, *J* = 8.1, 7.3 Hz, 1H), 6.72 (dd, *J* = 7.9, 7.3 Hz, 1H), 3.99–3.91 (m, 2H), 3.52 (s, 2H), 3.50–3.44 (m, 2H), 2.96–2.88 (m,

2H), 2.46–2.37 (m, 2H), 1.73–1.62 (m, 4H). ^{13}C NMR (100 MHz, DMSO-d_6) δ 172.6, 155.6, 150.3, 138.1, 136.1, 132.3, 127.0, 125.3, 124.8, 123.9, 120.8, 119.2, 118.4, 118.0, 115.3, 111.3, 111.1, 108.4, 48.6, 39.1, 32.6, 27.9, 23.4, 21.3, 20.2. ESI-MS *m/z* 399.2 $[M+H]^+$. HR-ESIMS: $[M+H]^+$ calcd for $C_{25}H_{27}N_4O^+$ 399.2179, found 399.2179.

*4.1.6.2. 2-(1H-Indol-3-yl)-N-(3-((1,2,3,4-tetrahydroacridin-9-yl)amino) propyl)acetamide (**5b**).* Yellow oil in 62.9% yield. mp 84.2–85.6 °C. HPLC purity: 96.5%, t_R = 13.61 min. ^{1}H NMR (600 MHz, DMSO-d_6) δ 10.88 (brs, 1H, NH), 8.12 (d, *J* = 8.5 Hz, 1H), 7.98 (t, *J* = 5.7 Hz, 1H, NH), 7.72 (d, *J* = 8.4 Hz, 1H), 7.54 (dd, *J* = 8.4, 7.0 Hz, 1H), 7.52 (d, *J* = 7.6 Hz, 1H), 7.34 (dd, *J* = 8.5, 7.0 Hz, 1H), 7.33 (d, *J* = 8.1 Hz, 1H), 7.18 (brs, 1H), 7.04 (dd, *J* = 8.1, 7.2 Hz, 1H), 6.92 (dd, *J* = 7.6, 7.2 Hz, 1H), 3.50 (s, 2H), 3.41–3.37 (m, 2H), 3.14–3.10 (m, 2H), 2.90 (t, *J* = 6.3 Hz, 2H), 2.66 (t, *J* = 6.3 Hz, 2H), 1.83–1.78 (m, 2H), 1.78–1.73 (m, 2H), 1.70–1.64 (m, 2H). ^{13}C NMR (150 MHz, DMSO-d_6) δ 171.1, 157.4, 150.6, 146.2, 136.1, 128.3, 127.6, 127.2, 123.8, 123.5, 123.0, 120.9, 119.9, 118.6, 118.3, 115.7, 111.3, 108.8, 45.0, 36.1, 33.1, 32.7, 30.7, 25.0, 22.7, 22.3. ESI-MS *m/z* 413.2 $[M+H]^+$. HR-ESIMS: $[M+H]^+$ calcd for $C_{26}H_{29}N_4O^+$ 413.2336, found 413.2330.

*4.1.6.3. 2-(1H-Indol-3-yl)-N-(4-((1,2,3,4-tetrahydroacridin-9-yl)amino) butyl)acetamide (**5c**).* Yellow oil in 62.3% yield. mp 98.4–100.2 °C. HPLC purity: 96.4%, t_R = 13.90 min. ^{1}H NMR (600 MHz, DMSO-d_6) δ 10.89 (brs, 1H, NH), 8.29 (d, *J* = 8.6 Hz, 1H), 7.96 (t, *J* = 5.6 Hz, 1H, NH), 7.87 (d, *J* = 8.3 Hz, 1H), 7.73 (dd, *J* = 8.3, 7.4 Hz, 1H), 7.51 (d, *J* = 7.9 Hz, 1H), 7.47 (dd, *J* = 8.6, 7.4 Hz, 1H), 7.31 (d, *J* = 8.1 Hz, 1H), 7.15 (brs, 1H), 7.02 (dd, *J* = 8.1, 7.2 Hz, 1H), 6.89 (dd, *J* = 7.9, 7.2 Hz, 1H), 3.71–3.65 (m, 2H), 3.46 (s, 2H), 3.08–3.02 (m, 2H), 2.97–2.93 (m, 2H), 2.67–2.62 (m, 2H), 1.84–1.76 (m, 4H), 1.68–1.61 (m, 2H), 1.48–1.40 (m, 2H). ^{13}C NMR (150 MHz, DMSO-d_6) δ 170.6, 153.9, 152.9, 140.7, 136.1, 131.1, 127.2, 124.5, 124.4, 123.7, 122.0, 120.9, 118.6, 118.2, 117.0, 112.6, 111.3, 108.9, 47.1, 38.2, 32.8, 29.7, 27.6, 26.4, 24.3, 21.9, 21.0. ESI-MS *m/z* 427.2 $[M+H]^+$. HR-ESIMS: $[M+H]^+$ calcd for $C_{27}H_{31}N_4O^+$ 427.2492, found 427.2491.

*4.1.6.4. 2-(1H-Indol-3-yl)-N-(5-((1,2,3,4-tetrahydroacridin-9-yl)amino) pentyl)acetamide (**5d**).* Yellow solid in 72.2% yield, mp 65.4–67.6 °C. HPLC purity: 95.1%, t_R = 14.67 min. ^{1}H NMR (600 MHz, DMSO-d_6) δ 10.92 (brs, 1H, NH), 8.37 (d, *J* = 8.5 Hz, 1H), 8.00–7.94 (m, 2H), 7.82 (dd, *J* = 8.4, 7.9 Hz, 1H), 7.53 (dd, *J* = 8.5, 7.9 Hz, 1H), 7.52 (d, *J* = 7.7 Hz, 1H), 7.31 (d, *J* = 8.1 Hz, 1H), 7.16 (brs, 1H), 7.01(dd, *J* = 8.1, 7.1 Hz, 1H), 6.91 (dd, *J* = 7.7, 7.1 Hz, 1H), 3.80–3.72 (m, 2H), 3.47 (s, 2H), 3.07–3.03 (m, 2H), 3.01–2.97 (m, 2H), 2.67–2.60 (m, 2H), 1.84–1.76 (m, 4H), 1.74–1.66 (m, 2H), 1.44–1.37 (m,2H), 1.32–1.27 (m, 2H). ^{13}C NMR (150 MHz, DMSO-d_6) δ 170.6, 155.4, 150.8, 138.3, 136.1, 132.3, 127.2, 125.0, 124.9, 123.7, 120.8, 119.5, 118.7, 118.1, 115.7, 111.3, 111.2, 109.0, 47.2, 38.3, 32.8, 29.5, 28.7, 28.1, 24.0, 23.4, 21.5, 20.3. ESI-MS *m/z* 441.2 $[M+H]^+$. HR-ESIMS: $[M+H]^+$ calcd for $C_{28}H_{33}N_4O^+$ 441.2649, found 441.2653.

*4.1.6.5. 2-(1H-Indol-3-yl)-N-(6-((1,2,3,4-tetrahydroacridin-9-yl)amino) hexyl)acetamide (**5e**).* Yellow solid in 62.3% yield, mp 70.5–72.3 °C. HPLC purity:95.5%, t_R = 15.18 min. ^{1}H NMR (600 MHz, DMSO-d_6) δ 10.88 (brs, 1H, NH), 8.16 (d, *J* = 8.5 Hz, 1H), 7.85 (t, *J* = 5.5 Hz, 1H, NH), 7.74 (d, *J* = 8.4 Hz, 1H), 7.58 (dd, *J* = 8.4, 7.7 Hz, 1H), 7.52 (d, *J* = 7.9 Hz, 1H), 7.37 (dd, *J* = 8.5, 7.7 Hz, 1H), 7.32 (d, *J* = 8.1 Hz, 1H), 7.16 (brs, 1H), 7.02 (dd, *J* = 8.1, 7.6 Hz, 1H), 6.91 (dd, *J* = 7.9, 7.6 Hz, 1H), 3.47 (s, 2H), 3.46–3.42 (m, 2H), 3.03–2.98 (m, 2H), 2.92 (t, *J* = 5.8 Hz, 2H), 2.68 (t, *J* = 5.4 Hz, 2H), 1.85–1.78 (m, 4H), 1.57–1.50 (m, 2H), 1.37–1.31 (m, 2H), 1.28–1.18 (m, 4H). ^{13}C NMR (150 MHz, DMSO-d_6) δ 170.5, 156.4, 151.4, 145.0, 136.1, 128.8, 127.2, 126.4, 123.7, 123.6, 123.5, 120.9, 119.3, 118.7, 118.2, 114.8, 111.3, 109.0, 47.7, 38.5, 32.8, 32.4, 30.4, 29.1, 26.1, 26.0, 24.9, 22.5, 22.0. ESI-MS *m/z* 455.2 $[M+H]^+$. HR-ESIMS: $[M+H]^+$ calcd for $C_{29}H_{35}N_4O^+$ 455.2805, found 455.2803.

*4.1.6.6. 2-(1H-Indol-3-yl)-N-(7-((1,2,3,4-tetrahydroacridin-9-yl)amino) heptyl)acetamide (**5f**).* Yellow oil in 42% yield. mp 74.3–75.4 °C. HPLC purity: 96.0%, t_R = 16.01 min. ^{1}H NMR (600 MHz, DMSO-d_6) δ 10.87 (brs, 1H, NH), 8.12 (d, *J* = 8.5 Hz, 1H), 7.82 (t, *J* = 5.5 Hz, 1H, NH), 7.71 (d, *J* = 8.4 Hz, 1H), 7.53 (dd, *J* = 8.4, 7.8 Hz, 1H), 7.52 (d, *J* = 7.5H, 1H), 7.34 (dd, *J* = 8.5, 7.8 Hz, 2H), 7.16 (brs, 1H), 7.04 (dd, *J* = 8.0, 7.3 Hz, 1H), 6.94 (dd, *J* = 7.5, 7.3 Hz, 1H), 3.47 (s, 2H), 3.42–3.37 (m, 2H), 3.02–2.97 (m, 2H), 2.90 (t, *J* = 6.1 Hz, 2H), 2.69 (t, *J* = 6.2 Hz, 2H), 1.85–1.75 (m, 4H), 1.56–1.49 (m, 2H), 1.37–1.29 (m, 2H), 1.26–1.17 (m, 6H). ^{13}C NMR (150 MHz, DMSO-d_6) δ 170.5, 157.4, 150.7, 146.3, 136.1, 128.2, 127.7, 127.2, 123.7, 123.3, 123.2, 120.9, 119.9, 118.7, 118.2, 115.5, 111.3, 109.0, 47.9, 38.5, 33.2, 32.8, 30.5, 29.1, 28.5, 26.3, 26.3, 25.0, 22.7, 22.3. ESI-MS *m/z* 469.2 $[M+H]^+$. HR-ESIMS: $[M+H]^+$ calcd for $C_{30}H_{37}N_4O^+$ 469.2962, found 469.2965.

*4.1.6.7. 2-(1H-Indol-3-yl)-N-(8-((1,2,3,4-tetrahydroacridin-9-yl)amino) octyl)acetamide (**5g**).* Yellow solid in 53.2% yield, mp 70.9–71.6 °C. HPLC purity: 95.4%, t_R = 17.16 min. ^{1}H NMR (400 MHz, DMSO-d_6) δ 10.92 (brs, 1H, NH), 8.31 (d, *J* = 8.6 Hz, 1H), 7.92 (t, *J* = 5.4 Hz, 1H, NH), 7.89 (d, *J* = 8.6 Hz, 1H), 7.74 (dd, *J* = 8.6, 7.4 Hz, 1H), 7.52 (d, *J* = 7.9 Hz, 1H), 7.49 (dd, *J* = 8.6, 7.4 Hz, 1H), 7.32 (d, *J* = 8.1 Hz, 1H), 7.16 (brs, 1H), 7.02 (dd, *J* = 8.1, 7.2 Hz, 1H), 6.92 (dd, *J* = 7.9, 7.2 Hz, 1H), 3.73–3.65 (m, 2H), 3.47 (s, 2H), 3.04–2.98 (m, 2H), 2.98–2.92 (m, 2H), 2.69–2.60 (m, 2H), 1.86–1.76 (m, 4H), 1.68–1.58 (m, 2H), 1.38–1.30 (m, 2H), 1.28–1.23 (m, 2H), 1.22–1.14 (m, 6H). ^{13}C NMR (100 MHz, DMSO-d_6) δ 170.5, 154.1, 152.5, 140.3, 136.1, 131.2, 127.2, 124.5, 124.4, 123.7, 121.7, 120.8, 118.7, 118.1, 116.8, 112.4, 111.3, 109.0, 47.4, 38.5, 32.8, 32.2, 30.0, 29.5, 29.1, 28.6, 26.2, 26.0, 24.3, 21.8, 20.9. ESI-MS *m/z* 483.2 $[M+H]^+$. HR-ESIMS: $[M+H]^+$ calcd for $C_{31}H_{39}N_4O^+$ 483.3118, found 483.3116.

4.2. AChE/BChE bioassay

AChE and BChE inhibitory activities of compounds were determined by using modified Ellman's method [37,38]. Electric eel AChE, equine serum BChE, 5,5′-dithiobis(2-nitrobenzoic acid) (DTNB), phosphate buffer solution (PBS, pH 8.0), acetylthiocholine (ATC) iodide, and butyrylthiocholine (BUC) iodide were purchased from Sigma-Aldrich (Steinheim, Germany). Tacrine was used as positive control. Enzyme solutions were prepared at 2.0 U/mL in 2 mL aliquots. The assay medium consisted of 10 μL of enzyme, 40 μL of PBS, 20 μL of 0.01 M DTNB and 10 μL of tested compound. Assayed solutions of tested compounds were pre-incubated with corresponding ChE for 5 min. The reaction was initiated by addition of 20 μL of 0.01 M substrate (ATC or BUC). The activity was determined by measuring the increase in absorbance at 410 nm at 37 °C in 2 min intervals using Tecan Spark multimode microplate reader (Mannedorf, Switzerland). The percentage of inhibition (*I*) was calculated from the measured data as follows: $I = (A_c - A_i)/A_c \times 100\%$, where A_i and A_c represent the change in the absorbance in the presence of inhibitor and without inhibitor, respectively.

4.3. Kinetic assay

Kinetic studies of inhibition on AChE and BChE were performed by using Ellman's method as described above. The concentrations of used substrates were 0.07813, 0.1563, 0.3125, and 0.625 μM. Linear regression was used for calculation of Lineweaver–Burk plots, and all the calculations were performed using GraphPad Prism 5.0 software.

4.4. Molecular docking

GLIDE 5.5 program [39,40] was employed to perform molecular docking studies. The LigPrep [41] panel was used to produce multiple

output structures of inhibitors by generating different protonation states, stereochemistry, tautomers, and ring conformations for molecular docking. The Protein Preparation Wizard Workflow was used to process and minimize the protein structures. Residues located within 20 Å around **AA7** on AChE (PDB: 5EI5) [17,42] and tacrine on BChE (4BDS) [43] were defined as binding sites in which the docking grids were created. The default settings were used. The inhibitors were docked into the defined binding site using extra precision (XP) mode without any constraint and were ranked by Glide-score.

4.5. Molecular dynamics simulation

Molecular dynamics (MD) simulations were performed on **1a**/AChE and **5e**/AChE complexes obtained from molecular docking. Before simulation, the protonation states of ionizable residues of AChE were determined using the H++ program [44]. Each complex model was surrounded by a periodic box of transferable intermolecular potential 3P [45] water molecules that extend 10 Å from the protein atoms. Counter-ions ($Na^+ \times 2$) were added to neutralize each simulation system. The parm99SB version of the all-atom assisted model building and energy refinement (AMBER) force field was used to represent the protein system. Atom types and charges of **1a** and **5e** were generated by antechamber package [46,47].

Firstly, energy minimization (8000 steps for the water molecules followed by 6000 steps for the whole system) for each solvated system was done to remove poor contacts between the solute and the solvent. All MD simulations were conducted using the SANDER program included in the AMBER package (version 10.0) [48] at constant temperature and pressure and periodic boundary conditions with a time step of 10 fs. The SHAKE algorithm [49] was used to constrain all hydrogen atom bonds. Electrostatic interactions were calculated using the particle-mesh Ewald method [50]. The non-bonded cutoff was set to 10.0 Å, and the non-bonded pairs were updated every 25 steps. The temperature (300 K) and pressure (1 atm = 101.3 kPa) of the system were controlled during the MD simulations by applying the algorithm developed by Berendsen et al. [51] The temperature and pressure coupling parameters were set to 1 ps.

4.6. Binding free energy calculation by MM-PBSA method

Based on the equilibrated dynamic trajectory, the binding free energy of each complex was calculated using the MM-PBSA method encoded in the AMBER 10.0 program. A total of 2000 snapshots from the trajectory were extracted every 50 ps, and the MM-PBSA calculation was performed on each snapshot using the MM-PBSA.PY module in AMBER 10.0.

4.7. Prediction of pharmacokinetic properties

The pharmacokinetic properties of these dual AChE/BChE inhibitors were predicted by the 'ADMET Descriptors' module implemented in DS3.0 [52]. The pharmacokinetic properties involved aqueous solubility, absorption, BBB, CYP2D6 binding and plasma protein binding.

4.8. Neural network electrical activity test

Primary mouse hippocampal cultures from newborn pups were generated as described previously [53]. Neurons were infected at 5 days old by lentivirus expressing GCaMP6 under human-synapsin I promoter. Lentivirus was produced in HEK293T cells by calcium phosphate transfection. Experiments were carried out when the cultures were 15–19 days old. For recording, neuronal cultures were placed in a recording chamber with extracellular solution containing (in mM): 140 NaCl, 5 KCl, 2 $CaCl_2$, 2 $MgCl_2$, 10 HEPES-NaOH, 10 glucose, pH 7.4 (310 mOsm). Images were taken using a custom-built epifluorescence microscopy with a CMOS camera (Thorlabs). Excitation light (0.2 mW/mm^2) was generated using a 470 nm LED (Thorlabs) and images were taken every 2.5 s for 2 h before and after adding the drug. A self-written Matlab program was produced to analyze the images. Briefly, individual neurons were first detected using Otsu's algorithm and by a size filter of 16–200 μm^2. The time courses of each cell were then generated and averaged, and physiological parameters were derived from the time courses.

Conflicts of interest

There are no conflicts to declare.

Acknowledgements

This research work was financially supported by the Natural Science Foundation of China [Nos. 21672082, 81803438], Shandong Key Development Project [No. 2016GSF201209], the Young Taishan Scholars Program [No. tsqn20161037], Natural Science Foundation of Shandong Province [No. ZR2017BH038, JQ201721, ZR2018ZC0944], and Shandong Talents Team Cultivation Plan of University Preponderant Discipline [No. 10027]. Authors are grateful to Jin-Tong Song (School of Biological Science and Technology, University of Jinan) for NMR analytical support.

References

[1] S. Thiratmatrakul, C. Yenjai, P. Waiwut, O. Vajragupta, P. Reubroycharoen, M. Tohda, C. Boonyarat, Eur. J. Med. Chem. 75 (2014) 21–30.
[2] < http://www.worldalzreport2015.org > (Date accessed on 15/09/2017).
[3] A.T. Kodamullil, F. Zekri, M. Sood, B. Hengerer, L. Canard, D. McHale, M. Hofmann-Apitius, Nat. Rev. Drug Discov. 16 (2017) 819.
[4] N.H. Greig, T. Utsuki, Q. Yu, X. Zhu, H.W. Holloway, T. Perry, B. Lee, D.K. Ingram, D.K. Lahiri, Curr. Med. Res. Opin. 17 (2001) 159–165.
[5] P.B. AnandSingh, Arch. Pharm. Res. 36 (2013) 375–399.
[6] B. Feng, X.-P. Li, J. Xia, S. Wu, J. Enzy. Inhib. Med. Chem. 32 (2017) 968–977.
[7] D. De Vita, F. Pandolfi, L. Ornano, M. Feroci, I. Chiarotto, I. Sileno, F. Pepi, R. Costi, R. Di Santo, L. Scipione, J. Enzyme. Inhib. Med. Chem. 31 (2016) 106–113.
[8] R.C. Petersen, R.G. Thomas, M. Grundman, D. Bennett, R. Doody, S. Ferris, D. Galasko, S. Jin, J. Kaye, A. Levey, E. Pfeiffer, M. Sano, C.H. van Dyck, L.J. Thal, N. Engl. J. Med. 352 (2005) 2379–2388.
[9] M. Weinstock, CNS Drugs 12 (2012) 307–323.
[10] N.H. Greig, T. Utsuki, D.K. Ingram, Y. Wang, G. Pepeu, C. Scali, Q.S. Yu, J. Mamczarz, H.W. Holloway, T. Giordano, D. Chen, K. Furukawa, K. Sambamurti, A. Brossi, D.K. Lahiri, Proc. Natl. Acad. Sci. USA 102 (2005) 17213–17218.
[11] K.V. Dileep, C. Remya, I. Tintu, C. Sadasivan, Front Life Sci. 7 (2013) 164–173.
[12] S. Darvesh, D. Hopkins, A.C. Geula, Nat. Rev. Neurosci. 4 (2003) 131–138.
[13] L. Ismaili, B. Refouvelet, M. Benchekroun, S. Brogi, M. Brindisi, S. Gemma, G. Campiani, S. Filipic, D. Agbaba, G. Esteban, M. Unzeta, K. Nikolic, S. Butini, J. Marco-Contelles, Prog. Neurobiol. 151 (2017) 4–34.
[14] N. Guzior, A. Wieckowska, D. Panek, B. Malawska, Curr. Med. Chem. 22 (2015) 373–404.
[15] C.S. Jiang, Y. Fu, L. Zhang, J.X. Gong, Z.Z. Wang, W. Xiao, H.Y. Zhang, Y.W. Guo, Bioorg. Med. Chem. Lett. 25 (2015) 216–220.
[16] J.C. Li, J. Zhang J, M.C. Rodrigues, D.J. Ding, L.P. Longo, R.B. Azevedo, L.A. Muehlmann, C.S. Jiang, Bioorg. Med. Chem. Lett. 26 (2016) 3881–3885.
[17] H. Zhang, C.S. Jiang, K.K. Zhu, Z.Q. Cheng, J.L. Song, Y. Li, Y. Fei, M.J. Li, X. Wang, CN107814787A, 2018.
[18] J.L. Sussman, M. Harel, F. Frolow, C. Oefner, A. Goldman, L. Toker, I. Silman, Science 253 (1991) 872–879.
[19] G. Koellner, T. Steiner, C.B. Millard, I. Silman, J.L. Sussman, J. Mol. Biol. 320 (2002) 721–725.
[20] S. Ölgen, F. Bakar, S. Aydin, D. Nebioğlu, S. Nebioğlu, J. Enzyme Inhib. Med. Chem. 28 (2013) 58–64.
[21] M.J. Uddin, B.C. Crews, K. Ghebreselasie, L.J. Marnett, Bioconjug Chem. 24 (2013) 712–723.
[22] Z. Li, J. Li, J. Liu, Z. Zhao, C. Xia, D. Li, ChemCatChem 6 (2014) 1333–1339.
[23] Z. Liu, L. Fang, H. Zhang, S. Gou, L. Chen, Bioorg. Med. Chem. 25 (2017) 2387–2398.
[24] L. Fang, D. Appenroth, M. Decker, M. Kiehntopf, A. Lupp, S. Peng, C. Fleck, Y. Zhang, J. Lehmann, J. Med. Chem. 51 (2008) 7666–7669.
[25] E. Nepovimova, J. Korabecny, R. Dolezal, K. Babkova, A. Ondrejicek, D. Jun, V. Sepsova, A. Horova, M. Hrabinova, O. Soukup, N. Bukum, P. Jost, L. Muckova, J. Kassa, D. Malinak, J.M. Andrs, K. Kuca, J. Med. Chem. 58 (2015) 8985–9003.
[26] J. Jeřábek, E. Uliassi, L. Guidotti, J. Korábečný, O. Souku, V. Sepsova, M. Hrabinova, K. Kuča, M. Bartolini, L.E. Peña-Altamira, S. Petralla, B. Monti, M. Roberti, M.L. Bolognesi, Eur. J. Med. Chem. 127 (2017) 250–262.
[27] E.H. Rydberg, B. Brumshtein, H.M. Greenblatt, D.M. Wong, D. Shaya, L.D. Williams, P.R. Carlier, Y.P. Pang, I. Silman, J.L. Sussman, J. Med. Chem. 49 (2006)

5491–5500.
[28] G.L. Delogu, M.J. Matos, M. Fanti, B. Era, R. Medda, E. Pieroni, A. Fais, A. Kumar, F. Pintus, Bioorg. Med. Chem. Lett. 26 (2016) 2308–2313.
[29] X. Pang, H. Fu, S. Yang, L. Wang, A.L. Liu, S. Wu, G.H. Du, Molecules 22 (2017) E1254.
[30] H. Pajouhesh, G.R. Lenz, NeuroRx 2 (2005) 541–553.
[31] G. Buzsáki, A. Draguhn, Science 304 (2004) 1926–1929.
[32] J.J. Palop, L. Mucke, Nat. Rev. Neurosci. 17 (2016) 777–792.
[33] J.F. Poulet, C.C. Petersen, Nature 454 (2008) 881–885.
[34] A. Ahnaou, H. Huysmans, T. Jacobs, W.H. Drinkenburg, Neuropharmacology 86 (2014) 362–377.
[35] Y. Penn, M. Segal, E. Moses, Proc. Natl. Acad. Sci. USA 113 (2016) 3341–3346.
[36] T.W. Chen, T.J. Wardill, Y. Sun, S.R. Pulver, S.L. Renninger, A. Baohan, E.R. Schreiter, R.A. Kerr, M.B. Orger, V. Jayaraman, L.L. Looger, K. Svoboda, D.S. Kim, Nature 499 (2013) 295–300.
[37] G.L. Ellman, K.D. Courtney, V. Andres, R.M. Feather-Stone, Biochem. Pharmacol. 7 (1961) 88–95.
[38] T.N. Talesa, Mech. Ageing Dev. 122 (2001) 1961–1969.
[39] R.A. Friesner, J.L. Banks, R.B. Murphy, T.A. Halgren, J.J. Klicic, D.T. Mainz, M.P. Repasky, E.H. Knoll, M. Shelley, J.K. Perry, D.E. Shaw, P. Francis, P.S. Shenkin, J. Med. Chem. 47 (2004) 1739–1749.
[40] T.A. Halgren, R.B. Murphy, R.A. Friesner, H.S. Beard, L.L. Frye, W.T. Pollard, J.L. Banks, J. Med. Chem. 47 (2004) 1750–1759.
[41] LigPrep, version 2.3; Schrödinger, LLC, New York, NY, 2009.
[42] http://www.rcsb.org/pdb/explore/explore.do?structureId=5ei5.
[43] F. Nachon, E. Carletti, C. Ronco, M. Trovaslet, Y. Nicolet, L. Jean, P.Y. Renard, Biochem. J. 453 (2013) 393–399.
[44] J.C. Gordon, J.B. Myers, T. Folta, V. Shoja, L.S. Heath, A. Onufriev, Nucleic Acids Res. 33 (2005) W368–W371.
[45] W.L. Jorgensen, J. Chandrasekhar, J.D. Madura, R.W. Impey, M.L. Klein, J. Chem. Phys. 79 (1983) 926–935.
[46] J. Wang, W. Wang, P.A. Kollman, D.A. Case, J. Mol. Graph. Model 25 (2006) 247–260.
[47] J. Wang, R.M. Wolf, J.W. Caldwell, P.A. Kollman, D.A. Case, J. Comput. Chem. 25 (2004) 1157–1174.
[48] D.A. Case, T.E. Cheatham 3rd, T. Darden, H. Gohlke, R. Luo, K.M. Merz Jr, A. Onufriev, C. Simmerling, B. Wang, R.J. Woods, J. Comput. Chem. 26 (2005) 1668–1688.
[49] J.P. Ryckaert, G. Ciccotti, H.J.C. Berendsen, J. Comput. Phys. 23 (1997) 327–341.
[50] T. Darden, D. York, L. Pedersen, J. Chem. Phys. 98 (1993) 10089–10092.
[51] H.J.C. Berendsen, J.P.M. van Postma, W.F. van Gunsteren, A. DiNola, J.R. Haak, J. Chem. Phys. 81 (1984) 3684–3690.
[52] Accelrys Discovery Studio 3.0, Accelrys, San Diego, CA, 2010.
[53] C. Liu, L.S. Bickford, R.G. Held, H. Nyitrai, T.C. Südhof, P.S. Kaeser, J. Neurosci. 34 (2014) 12289–12303.